Physics of Fluids

Evolutions of strain rate and dissipation rate of kinetic energy in turbulent premixed flames

Cite as: Phys. Fluids **33**, 125132 (2021); https://doi.org/10.1063/5.0076373
Submitted: 24 October 2021 • Accepted: 06 December 2021 • Published Online: 28 December 2021

Nilanjan Chakraborty, Christian Kasten, Umair Ahmed, et al.

Physics of Fluids ARTICLE scitation.org/journal/phf

Evolutions of strain rate and dissipation rate of kinetic energy in turbulent premixed flames

Cite as: Phys. Fluids 33, 125132 (2021); doi: 10.1063/5.0076373
Submitted: 24 October 2021 · Accepted: 6 December 2021 ·
Published Online: 28 December 2021

View Online Export Citation CrossMark

Nilanjan Chakraborty,[1] Christian Kasten,[2] Umair Ahmed,[1] and Markus Klein[2,a)]

AFFILIATIONS

[1]School of Engineering, University of Newcastle, Claremont Road, Newcastle NE1 7RU, United Kingdom
[2]Department of Aerospace Engineering, Bundeswehr University Munich, Werner-Heisenberg-Weg 39, 85577 Neubiberg, Germany

[a)]Author to whom correspondence should be addressed: markus.klein@unibw.de

ABSTRACT

The statistical behaviors of the evolutions of the components of the strain rate tensor and Favre-averaged dissipation rate of kinetic energy are analyzed using direct numerical simulations of statistically planar turbulent premixed flames propagating into forced unburned gas turbulence for different turbulence intensities spanning a range of different Karlovitz numbers. The pressure Hessian contribution and the combined molecular diffusion and dissipation terms are found to play dominant roles in the transport equations of diagonal strain rate components and the Favre-averaged dissipation rate of kinetic energy for flames with small Karlovitz numbers. By contrast, the leading order balance is maintained between the strain rate, vorticity, and molecular dissipation contributions for flames with large Karlovitz numbers, similar to non-reacting turbulent flows. The contributions of the terms arising from the correlation between pressure and density gradients and pressure Hessian in the strain rate and dissipation rate of kinetic energy transport equations weaken in comparison to the magnitude of the molecular dissipation contribution with an increase in Karlovitz number. These behaviors have been explained in terms of the alignments of vorticity, pressure gradient, and pressure Hessian eigenvectors with strain rate eigendirections. The magnitudes of the terms in the transport equation of the Favre-averaged dissipation rate of kinetic energy are also found to increase with increasing Karlovitz number, which is explained with the help of a detailed scaling analysis. This scaling analysis also explains the leading order contributions to the dissipation rate of kinetic energy for different combustion regimes.

I. INTRODUCTION

Turbulent premixed combustion has practical applications in automotive (e.g., spark ignition) engines and industrial gas turbines (e.g., lean premixed prevaporized gas turbine combustors), and, therefore, several analyses focused on its physical understanding and a detailed review of the current state of the art can be obtained from the monograph by Peters[1] or the review papers by Veynante and Vervisch.[2] However, there are still several unresolved challenges in the analysis of turbulent premixed combustion due to its nonlinear multiscale nature, which translates to several alternative modeling methodologies.[3] High pressure and flame instabilities pose additional modeling challenges.[4] The state of the art has been reviewed in several recent collections[5] or review papers dealing with turbulent flame speed and thickness,[6] turbulent transport,[7] and thermal expansion effects,[8] as well as the turbulent flame structure.[9,10] A key aspect in turbulent premixed flames is the heat release due to chemical reaction, which gives rise to thermal expansion, which is manifested by the predominantly positive values of the dilatation rate (i.e., $\partial u_i/\partial x_i \neq 0$ where u_i is the ith component of the fluid velocity). This has an important influence on the evolutions of turbulent kinetic energy,[11–15] enstrophy,[16–20] and scalar gradient[21–24] within the flame brush. Moreover, thermal expansion due to heat release in turbulent premixed flames has been demonstrated to influence the alignment of the vorticity[16] and scalar gradient[21–23] with local principal strain rates, and the alignment depends also on the Karlovitz (or Damköhler) number.[16,21] Furthermore, it has been found that the strength of thermal expansion can affect the relative alignment of sub-grid stresses with resolved strain rates, which can have implications on the sub-grid turbulent kinetic energy production in turbulent premixed combustion.[25] Interested readers are referred to a recent review[8] for a detailed discussion on the effects of heat release and thermal expansion on these aspects, and their implications on the modeling of turbulent premixed combustion. However, a relatively limited effort[26,27] has been directed to strain rate $S_{ij} = 0.5(\partial u_i/\partial x_j + \partial u_j/\partial x_i)$ transport in the context of turbulent

premixed combustion despite its importance in vortex-stretching and flame normal strain rate contributions to the enstrophy[16–20] and flame surface density (FSD)/scalar dissipation rate (SDR) transports.[28–33] Moreover, S_{ij} is closely linked to the dissipation rate of kinetic energy[2] $E = 2\nu S_{ij}S_{ij} - 2\nu S_{ii}S_{jj}/3$ where ν is the kinematic viscosity. Dissipation of (turbulent) kinetic energy is among the most important variables for the purpose of the closure of unknown correlations/terms, for isothermal flow as well as turbulent non-premixed and premixed flames as indicated by several recent analyses.[34–38] The most famous two-equation model solves a transport equation for dissipation of turbulent kinetic energy and the same holds true for Reynolds stress-based modeling. However, this equation is also unclosed and, thus, requires modeling. Furthermore, the dilatation rate $S_{ii} = \partial u_i/\partial x_i$ plays a key role in turbulent kinetic energy,[11–15] enstrophy,[17–19] and FSD/SDR[28–33,39] transports. Nomura and Post[40] analyzed the statistical behaviors of the terms of the principal strain rate transport equation for non-reacting turbulent flows under homogeneous isotropic turbulence. This analysis identified local and non-local contributions to the principal strain rate evolution and the generation of principal strain rates were found to be balanced by the viscous dissipation process. Steinberg *et al.*[26] used the combined planar laser induced fluorescence (PLIF) and particle image velocimetry (PIV) to analyze the statistical behaviors of the different terms of the principal strain rate transport equation for a piloted jet premixed flame under high Karlovitz number conditions. It has been found that the terms arising from pressure and density gradients play key roles in the evolution of the most extensive principal strain rate, but the influence of these terms remains weak for the evolution of the intermediate principal strain rate. The present authors[27] also analyzed the statistical behaviors of the different terms of principal strain rate transport equations for different turbulence intensities and Karlovitz numbers based on direct numerical simulations (DNS) of statistically planar turbulent premixed flames subjected to forced unburned gas turbulence. This analysis[27] suggested that the terms arising from pressure gradient and pressure Hessian play important roles in the evolution of principal strain rates for small values of the Karlovitz number, and the contributions of these terms diminish with the increasing Karlovitz numbers. Consequently, due to the definition of the dissipation rate of turbulent kinetic energy, the Karlovitz number is expected to affect its transport. This is also evident from the fact that the dissipation rate of turbulent kinetic energy depends on the turbulent Reynolds number Re_t, which scales with the product of the Damköhler number and Karlovitz number squared (i.e., $Re_t \sim Da^2Ka^2$).[1] However, to date, there have not been any analyses which focused on the evolutions of individual components of the strain rate tensor S_{ij} and their implications on the evolution of dissipation rate of kinetic energy E. The present analysis addresses the aforementioned gap in the existing literature by using a three-dimensional DNS dataset of statistically planar turbulent premixed flames representing different regimes of premixed combustion. In this respect, the main objectives of the current analysis are (a) to demonstrate the statistical behaviors of the different terms of the transport equation of the individual components of the strain rate tensor S_{ij}, (b) to demonstrate the effects of turbulence intensity and Karlovitz number on the statistical behaviors of the different terms of the transport equations of strain rate and the Favre-averaged dissipation rate of kinetic energy, and (c) to provide physical explanations for the observed behaviors.

II. MATHEMATICAL BACKGROUND AND NUMERICAL IMPLEMENTATIONS

The transport equation of S_{ij} can be derived by taking spatial derivatives of both sides of the momentum conservation equation $\left[\partial u_i/\partial t + u_j\partial u_i/\partial x_j\right] = \rho^{-1}[-\partial p/\partial x_i + \partial\tau_{ij}/\partial x_j]$ where ρ is the gas density and $\tau_{ij} = 2\rho\nu S_{ij} - 2\rho\nu\delta_{ij}S_{kk}/3$ is the component of the viscous stress tensor with δ_{ij} and $\nu = \mu/\rho$ being the Kronecker's delta and kinematic viscosity, respectively, and μ is the dynamic viscosity. For compressible flow, the transport equation of S_{ij} takes the following form:

$$\frac{\partial S_{ij}}{\partial t} + u_k\frac{\partial S_{ij}}{\partial x_k} = \underbrace{-S_{ik}S_{kj}}_{G_1^{ij}} \underbrace{-\left(\omega_i\omega_j - \delta_{ij}\omega_k\omega_k\right)/4}_{G_2^{ij}} + \underbrace{\frac{1}{2\rho^2}\left(\frac{\partial p}{\partial x_i}\frac{\partial \rho}{\partial x_j} + \frac{\partial p}{\partial x_j}\frac{\partial \rho}{\partial x_i}\right)}_{G_3^{ij}} \underbrace{-\frac{1}{\rho}\frac{\partial^2 p}{\partial x_i\partial x_j}}_{G_4^{ij}} \underbrace{-\frac{1}{2\rho^2}\left(\frac{\partial \tau_{ik}}{\partial x_k}\frac{\partial \rho}{\partial x_j} + \frac{\partial \tau_{jk}}{\partial x_k}\frac{\partial \rho}{\partial x_i}\right)}_{G_5^{ij}} + \underbrace{\frac{1}{2\rho}\left(\frac{\partial^2 \tau_{ik}}{\partial x_j\partial x_k} + \frac{\partial^2 \tau_{jk}}{\partial x_i\partial x_k}\right)}_{G_6^{ij}}, \tag{1}$$

where $\omega_i = \epsilon_{ijk}\partial u_k/\partial x_j$ is the ith component of vorticity, ϵ_{ijk} represents the Levi-Civita symbol, and p is the pressure. The two terms on the left-hand side of Eq. (1) are transient [i.e., partial time (t) derivative] and advection terms, respectively. The term G_1^{ij} accounts for the strain rate contribution to the evolution of S_{ij}, whereas the term G_2^{ij} is the vorticity contribution to the S_{ij} transport. The term G_3^{ij} arises due to the correlation between density and pressure gradients, whereas G_4^{ij} is the pressure Hessian contribution to the strain rate transport. The term G_5^{ij} originates due to density gradient and its correlation with the viscous stress gradient, whereas G_6^{ij} represents the combined contributions of molecular diffusion and molecular dissipation. From Eq. (1), it is possible to obtain a transport of the dilatation rate $S_{ii} = \partial u_i/\partial x_i$ in the following manner:

$$\frac{\partial S_{ii}}{\partial t} + u_k\frac{\partial S_{ii}}{\partial x_k} = \underbrace{-S_{ik}S_{ki}}_{G_1^{ii}} + \underbrace{\frac{(\omega_i\omega_i)}{2}}_{G_2^{ii}} + \underbrace{\frac{1}{\rho^2}\left(\frac{\partial p}{\partial x_i}\frac{\partial \rho}{\partial x_i}\right)}_{G_3^{ii}} \underbrace{-\frac{1}{\rho}\frac{\partial^2 p}{\partial x_i\partial x_i}}_{G_4^{ii}} \underbrace{-\frac{1}{\rho^2}\left(\frac{\partial \tau_{ik}}{\partial x_k}\frac{\partial \rho}{\partial x_i}\right)}_{G_5^{ii}} + \underbrace{\frac{1}{\rho}\left(\frac{\partial^2 \tau_{ik}}{\partial x_i\partial x_k}\right)}_{G_6^{ii}}. \tag{2}$$

Multiplying Eq. (1) $\times\, 4\mu S_{ij}$ yields

$$\frac{\partial(2\rho\nu S_{ij}S_{ij})}{\partial t} + \frac{\partial(2\rho u_k\nu S_{ij}S_{ij})}{\partial x_k} = 4\mu S_{ij}G_1^{ij} + 4\mu S_{ij}G_2^{ij} + 4\mu S_{ij}G_3^{ij} + 4\mu S_{ij}G_4^{ij} + 4\mu S_{ij}G_5^{ij} + 4\mu S_{ij}G_6^{ij} + 2\rho S_{ij}S_{ij}\left(\frac{D\nu}{Dt}\right), \tag{3}$$

where $D\nu/Dt = \partial\nu/\partial t + u_i\partial\nu/\partial x_i$ is the material derivative of kinematic viscosity. Similarly, multiplying Eq. (2) $\times\, 4\mu S_{jj}/3$ gives rise to

$$\frac{\partial\left(2\rho\nu S_{ii}S_{jj}/3\right)}{\partial t}+\frac{\partial\left(2\rho u_k\nu S_{ii}S_{jj}/3\right)}{\partial x_k} = 4\mu S_{jj}G_1^{ii}/3+4\mu S_{jj}G_2^{ii}/3+4\mu S_{jj}G_3^{ii}/3+4\mu S_{jj}G_4^{ii}/3 + 4\mu S_{jj}G_5^{ii}/3+4\mu S_{jj}G_6^{ii}/3+2\rho S_{ii}S_{jj}(D\nu/Dt)/3. \quad (4)$$

Subtracting Eq. (4) from Eq. (3) leads to a transport equation of E,

$$\frac{\partial(\rho E)}{\partial t}+\partial\frac{(\rho u_k E)}{\partial x_k}=T_I+T_{II}+T_{III}+T_{IV}+T_V+T_{VI}+\rho\nu^{-1}E\frac{D\nu}{Dt}, \quad (5)$$

where $T_\alpha = 4\mu[G_\alpha^{ij}S_{ij} - G_\alpha^{ii}S_{jj}/3]$ for $\alpha = I, II, III, IV, V,$ and VI. Reynolds averaging Eq. (5) provides

$$\frac{\partial\left(\overline{\rho}\tilde{E}\right)}{\partial t}+\frac{\partial\left(\overline{\rho u_k E}\right)}{\partial x_k} = \underbrace{\overline{T_I}}_{T_1}+\underbrace{\overline{T}_{II}}_{T_2}+\underbrace{\overline{T}_{III}}_{T_3}+\underbrace{\overline{T}_{IV}}_{T_4}+\underbrace{\overline{T}_V}_{T_5}+\underbrace{\overline{T}_{VI}}_{T_6}+\overline{\rho\nu^{-1}E\frac{D\nu}{Dt}}, \quad (6)$$

where $\overline{Q}$, $\tilde{Q} = \overline{\rho Q}/\overline{\rho}$, and $Q'' = Q - \tilde{Q}$ are the Reynolds-averaged, Favre-averaged values, and Favre fluctuation of a general variable Q, respectively. The last term on the right-hand side is dependent on the assumptions made regarding molecular transport and is often neglected. It has been checked that indeed this term is small compared to $T_1 - T_6$ for small turbulence intensity and negligible for higher turbulence intensity. Hence, the same approach has been adopted for the current analysis. It is important to note that the terms T_3 and T_5 do not appear in incompressible non-reacting flows.

In the context of Reynolds-averaged Navier–Stokes (RANS) simulations, $\tilde{E}$ can be expressed as $\tilde{E} = \left[\overline{2\rho\nu S_{ij}S_{ij}} - \overline{2\rho\nu S_{ii}S_{jj}}/3\right]/\overline{\rho} \approx \left[\overline{2\rho\nu S''_{ij}S''_{ij}} - \overline{2\rho\nu S''_{ii}S''_{jj}}/3\right]/\overline{\rho} = \tilde{\varepsilon}$ (because $2\overline{\rho}\tilde{\nu}\tilde{S}_{ij}\tilde{S}_{ij} \ll \overline{2\rho\nu S''_{ij}S''_{ij}}$ and $2\overline{\rho}\tilde{\nu}\tilde{S}_{ii}\tilde{S}_{jj} \ll \overline{2\rho\nu S''_{ii}S''_{jj}}$) where $\tilde{\varepsilon}$ is the dissipation rate of turbulent kinetic energy $\tilde{k} = 0.5\overline{\rho u''_i u''_i}/\overline{\rho}$.[12,41] Thus, Eq. (6) can also be considered as the transport equation of the dissipation rate of turbulent kinetic energy in the context of RANS. Therefore, the statistical behaviors of the terms $\{T_1, T_2, \ldots, T_6\}$ provide insights into the behaviors of the unclosed terms in the $\tilde{\varepsilon}$ transport equation.

The statistical behaviors of G_α^{ij} for $\alpha = I, II, III, IV, V$ and VI and $\{T_1, T_2, \ldots, T_6\}$ have been analyzed using an existing DNS database of statistically planar turbulent premixed flames subjected to forced unburned gas turbulence. Detailed descriptions of the numerical implementations pertaining to this DNS database have been provided elsewhere[25,27,42,43] and thus only a brief description has been provided here. The simulations have been carried out using a well-known DNS code SENGA+ where the conservation equations of mass, momentum, energy and species are solved in non-dimensional form. In SENGA+, high-order finite-difference (10th order for internal points and the order of accuracy gradually drops to a one-sided second order scheme at the non-periodic boundaries) and Runge–Kutta (third order) schemes are used for spatial discretization and explicit time advancement, respectively. A 10th order central difference scheme yields almost identical accuracy as that of a spectral scheme.[44] A skew-symmetric form is used for the convective terms to minimize the spatial coherence of the discretization error.[45] Further, the grid spacing ensures at least 10 grid points within the thermal flame thickness δ_{th} and 1.5 grid points within the Kolmogorov scale η. The PDF of turbulent non-reacting velocity field is approximately Gaussian but the deviation from a Gaussian distribution can be obtained at small length scales, which is consistent with previous findings.[46] Moreover, the PDFs of the velocity derivatives deviate from a Gaussian distribution and the tails of longitudinal as well as transverse velocity derivative PDFs are characterized by exponential distributions. However, the lateral derivative skewness is close to zero due to the symmetry of the Navier–Stokes equations. Moreover, the skewness S_k and kurtosis F_k for forced homogeneous isotropic turbulence are found to be $-0.6 \leq S_k \leq -0.35$ and $3.30 \leq F_k \leq 4.0$, which are consistent with previous experimental[47,48] and numerical[46,49] results. These findings for the current code and the numerical schemes used in this paper have been reported elsewhere (see Fig. 11 of Ref. 50) and thus are not repeated here, but interested readers are referred to Ref. 50 for further information.

The boundaries in the direction of mean flame propagation direction (i.e., x_1- direction) are taken to be turbulent inflow and partially nonreflecting outflow, respectively. The transverse boundaries (i.e., boundaries in x_2- and x_3-directions) are taken to be periodic. The boundary conditions are specified following the Navier–Stokes characteristics boundary conditions technique. A modified bandwidth forcing[50] is used to force turbulence in the unburned gas ahead of the flame so that both the root mean square turbulent velocity and integral length scale of turbulence can be maintained within the unburned gas. A single-step Arrhenius type irreversible chemical reaction is assumed for these simulations and the thermophysical parameters are chosen to represent the stoichiometric methane-air flame preheated to 415 K, which leads to a heat release parameter $\tau = (T_{ad} - T_0)/T_0 = 4.5$ where T_0 and T_{ad} are the unburned gas temperature and the adiabatic flame temperature, respectively. This simplification allows for an extensive parametric analysis and does not affect the conclusions of this investigation,[51] as the current analysis focuses on the aspects of fluid dynamics.

The mean inlet velocity U_{mean} is gradually modified to match the turbulent flame speed to ensure a statistically stationary state of the flame. The simulation domain for statistically planar turbulent premixed flames is taken to be $79.5\delta_{th} \times (39.8\delta_{th})^2$, which is discretized by a uniform Cartesian grid of dimension $800 \times 400 \times 400$ with $\delta_{th} = (T_{ad} - T_0)/\max|\nabla T|_L$ being the thermal flame thickness where T is the dimensional temperature. The root mean square turbulent velocity fluctuation (i.e., $u' = \sqrt{2k_{domain}/3}$) normalized by the unstrained laminar burning velocity u'/S_L and integral length scale to thermal flame thickness ratio l/δ_{th} are listed in Table I along with the values of Damköhler number $Da = lS_L/u'\delta_{th}$ and Karlovitz number $Ka = (u'/S_L)^{3/2}(l/\delta_{th})^{-1/2}$ where k_{domain} is the turbulent kinetic energy evaluated over the whole domain. The Damköhler number Da provides the ratio of the integral timescale or eddy turnover time $t_e = l/u'$ to the chemical timescale $t_c = \delta_{th}/S_L$. By contrast the Karlovitz number Ka corresponds to the smallest Kolmogorov eddies and is the ratio of the chemical timescale to the Kolmogorov timescale.[2] It is noted that a decrease in Da is associated with an increase in Ka and *vice versa* and they can be related to each other using the scaling relation $Re_t \sim Da^2Ka^2$.[1] As a consequence, the flame structure

TABLE I. The attributes of the DNS database considered for this analysis.

Cases	u'/S_L	l/δ_{th}	Da	Ka	Regime
A	1.0	3.0	3.0	0.58	Wrinkled/corrugated flamelets
B	3.0	3.0	1.0	3.0	Thin reaction zones
C	5.0	3.0	0.6	6.5	Thin reaction zones
D	7.5	3.0	0.4	11.9	Thin reaction zones
E	10.0	3.0	0.3	18.3	Thin reaction zones

cannot be described by only one parameter, and one needs to consider different flame structures and modeling strategies[2] depending on the question if turbulent eddies can or cannot enter the preheat and or reaction zone. The regimes of combustion for these cases are also indicated in Table I, which shows that the cases considered here range from the wrinkled/corrugated flamelets to the high Karlovitz number thin reaction zones regime.[1] The total simulation time for all cases remains greater than one through pass time and at least 10 eddy turnover times (i.e., $10l/u'$) to ensure a statistically steady state in all cases.[25,27,42,43]

For the purpose of evaluating the Reynolds-/Favre-averaged values of the quantity under consideration, it is ensemble averaged in the homogeneous directions (which are the transverse directions normal to the mean flame propagation direction in the current configuration) following previous studies[11–15] and also in time once the quasi-steady state has been obtained.

III. RESULTS AND DISCUSSION

The distributions of the normalized squared strain rate magnitude $S_{ij}S_{ij} \times \delta_{th}^2/S_L^2$ in the central-midplane for cases A, C, and E are shown in Figs. 1(a)–1(c), respectively. The contours of reaction progress variable $c = 0.1, 0.3, 0.5, 0.7,$ and 0.9, where c is defined in terms of a suitable reactants mass fraction Y_R as $c = (Y_{R0} - Y_R)/(Y_{R0} - Y_{R\infty})$ with the subscripts 0 and ∞ refering to values in unburned reactants and fully burned products. The DNS cases considered here exhibit a monotonic trend from case A to case E, and therefore, cases B and D are not explicitly shown in these and subsequent figures. It can be seen from Figs. 1(a)–1(c) that the distribution of $S_{ij}S_{ij}$ changes from case A to case E with the change in Ka. Further, high values of $S_{ij}S_{ij}$ are obtained within the flame in case A and the values within the flame are much greater than those in both unburned and burned gases. This behavior changes significantly with an increase in Ka. By contrast, in cases C and E, the magnitude of $S_{ij}S_{ij}$ decreases from the unburned gas to the burned gas side and this trend strengthens with increasing Ka. Moreover, Figs. 1(b) and 1(c) reveal that $S_{ij}S_{ij}$ values change sharply from high to low magnitudes, and the length scale over which $S_{ij}S_{ij}$ values change is smaller in case E than in case C. An increase in u'/S_L for a given value of l/δ_{th} increases the turbulent Reynolds number and thus the range of length scales observed in case E is greater than in case C.

The normalized mean values of $\{S_{11}, S_{22}, S_{12}, S_{23},$ and $\partial u_i/\partial x_i = S_{ii}\} \times \delta_{th}/S_L$ conditional upon c for cases A, C, and E are shown in Figs. 2(a)–2(c), respectively. As S_{33} and S_{13} are statistically similar to S_{22} and S_{12}, respectively, the mean values of S_{33} and S_{13} are

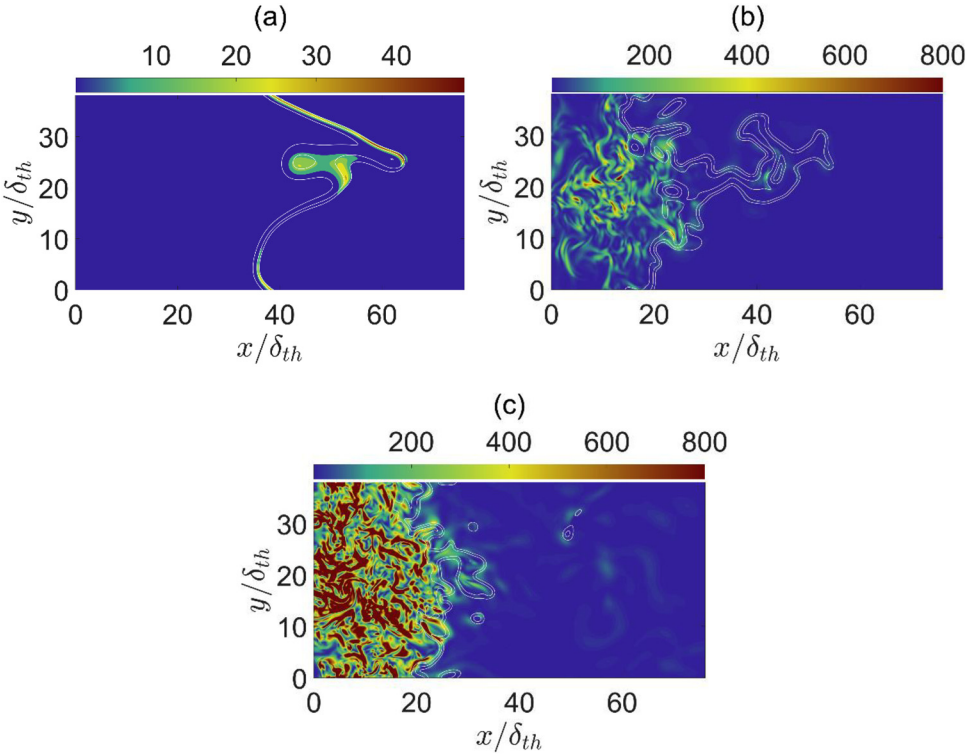

FIG. 1. Distributions of $S_{ij}S_{ij} \times \delta_{th}^2/S_L^2$ in the central midplane with $c = 0.1, 0.3, 0.5, 0.7, 0.9$ (left to right) superimposed for cases (a) A, (b) C, and (c) E.

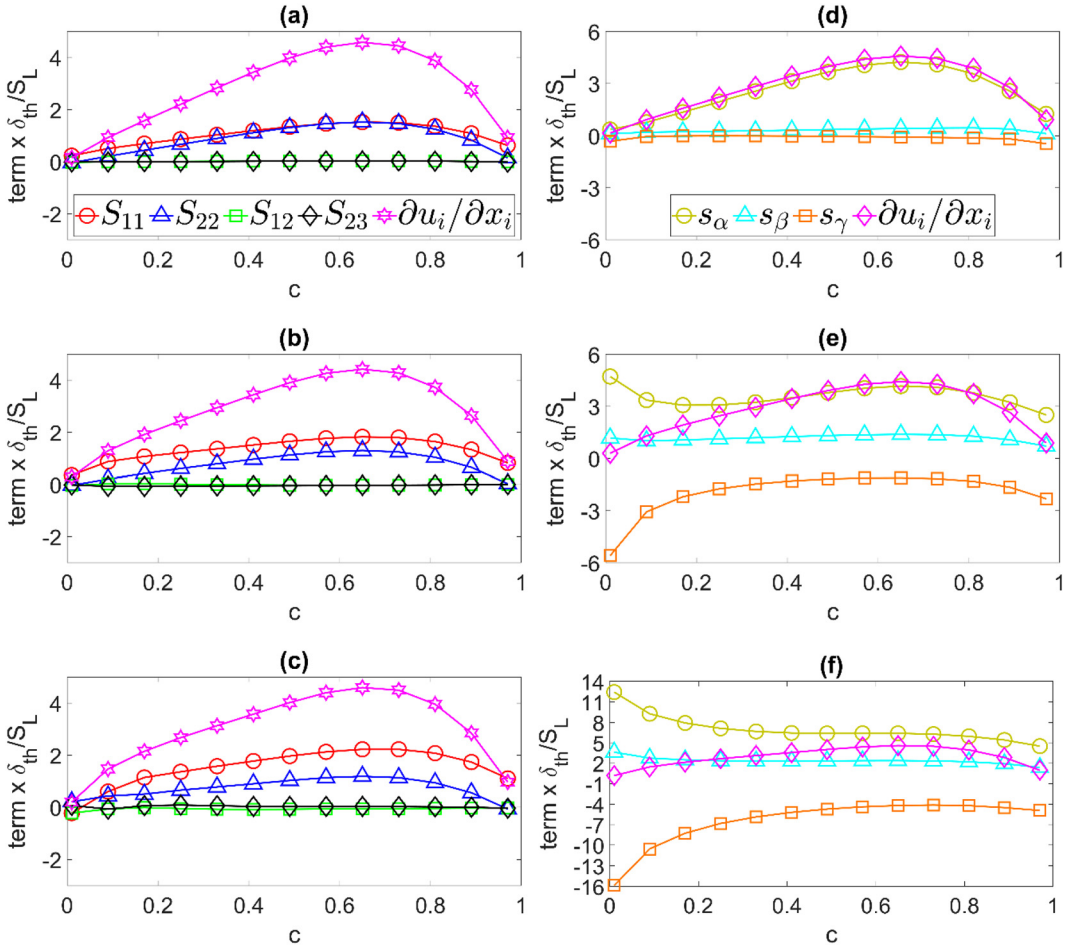

FIG. 2. Variations of the mean values of $\{S_{11}, S_{22}, S_{12}, S_{23}, \partial u_i/\partial x_i\} \times \delta_{th}/S_L$ (first column) and $\{s_\alpha, s_\beta, s_\gamma, \partial u_i/\partial x_i\} \times \delta_{th}/S_L$ (second column) conditioned upon c for cases (a) (d) A, (b) (e) C, and (c) (f) E.

not explicitly shown in Fig. 2 for the sake of brevity. It can be seen from Fig. 2 that the mean values of the diagonal components of strain rate tensor S_{11} and S_{22} are of comparable magnitudes and they remain much greater than the mean values of non-diagonal components S_{12} and S_{23} for all cases.

The trace of strain rate tensor S_{ii} provides the dilatation rate $\partial u_i/\partial x_i$ (i.e., $\partial u_i/\partial x_i = S_{ii}$) and its mean assumes positive values, and they are comparable for all cases because the mean value of dilatation rate conditional upon c are principally governed by the thermochemistry, which remains unaltered for all cases considered here. For the purpose of completeness, the normalized mean values of the strain rate eigenvalues $\{s_\alpha, s_\beta$ and $s_\gamma\} \times \delta_{th}/S_L$ (where s_α, s_β, and s_γ are the most extensive, intermediate, and the most compressive principal strain rates, respectively) conditional upon c are also shown in Figs. 2(d)–2(f). Although the mean values of $\partial u_i/\partial x_i = (s_\alpha + s_\beta + s_\gamma)$ remain comparable for all cases, the magnitudes of s_α and s_γ increase from case A to case C. In case A, the mean value of s_α remains much greater than those of s_β and s_γ and is almost equal to the mean value of $\partial u_i/\partial x_i$. However, the magnitudes of the mean value of s_α and s_γ become increasingly comparable moving from case A to case E and the mean values of strain rate eigenvalues follow $|\langle s_\gamma \rangle| > \langle s_\alpha \rangle > \langle s_\beta \rangle$ for cases C–E where $\langle Q \rangle$ is the mean value of a general quantity Q conditional upon c.

It is useful to analyze the evolutions of the individual components of the strain rate tensor S_{ij} within the flame in order to explain the observed differences in the distributions of $S_{ij}S_{ij} \times \delta_{th}^2/S_L^2$ and $S_{ij} \times \delta_{th}/S_L$ in Figs. 1 and 2, respectively. The normalized mean values of the terms on the right side of the transport equations of diagonal strain rate components S_{11} and S_{22} (i.e., $\{G_1^{11}, G_2^{11}, G_3^{11}, G_4^{11}, G_5^{11}, G_6^{11}\} \times \delta_{th}^2/S_L^2$ and $\{G_1^{22}, G_2^{22}, G_3^{22}, G_4^{22}, G_5^{22}, G_6^{22}\} \times \delta_{th}^2/S_L^2$) conditioned upon c for cases A, C, and E are shown in Figs. 3 and 4, respectively. The terms of the transport equation of S_{33} are both qualitatively and quantitatively same as that of S_{22} because x_2 and x_3 directions are statistically identical for the canonical configuration considered here. Thus, the terms of the transport equation of S_{33} are not explicitly shown for the sake of conciseness.

It can be seen from Figs. 3 and 4 that the strain rate contributions $G_1^{11} = -(S_{11}S_{11} + S_{12}S_{12} + S_{13}S_{13})$ and $G_1^{22} = -(S_{12}S_{12} + S_{22}S_{22} + S_{23}S_{23})$ assume negative mean values, as dictated by their mathematical expressions. The mean values of the vorticity contributions

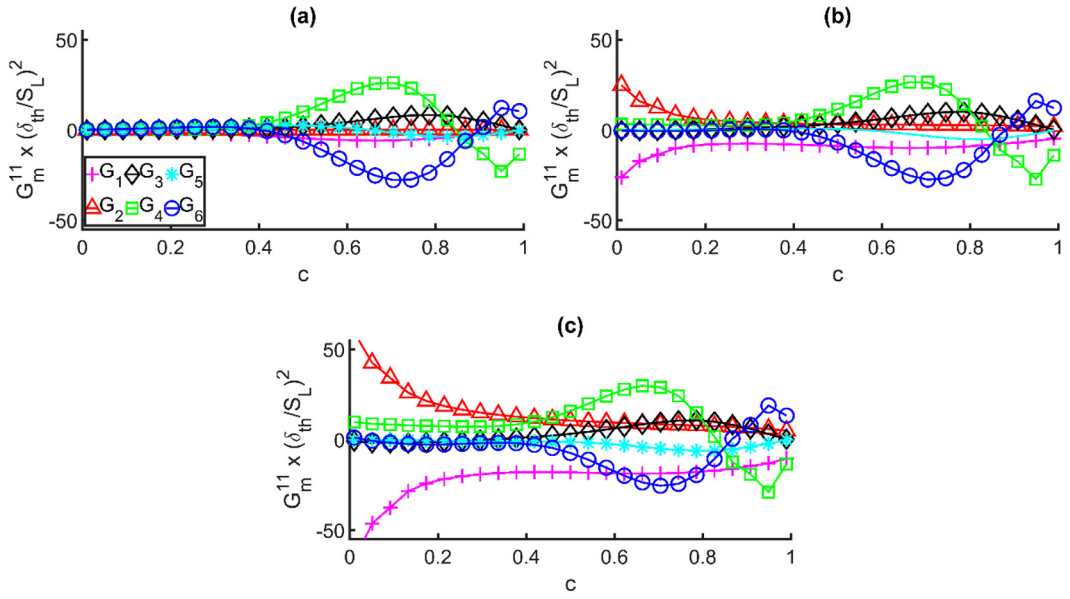

FIG. 3. Variations of the mean values of $\{G_1^{11}, G_2^{11}, G_3^{11}, G_4^{11}, G_5^{11}, G_6^{11}\} \times \delta_{th}^2/S_L^2$ conditioned upon c for cases (a) A, (b) C, and (c) E.

$G_2^{11} = (\omega_2\omega_2 + \omega_3\omega_3)/4$ and $G_2^{22} = (\omega_1\omega_1 + \omega_3\omega_3)/4$ remain small in case A (i.e., for small Karlovitz number flames) but its magnitude and relative strength increases with increasing Ka and becomes the leading source term for cases C–E where the magnitude of the positive values decreases from the unburned to the burned gas side of the flame front.

The magnitude of vorticity increases with the increasing u'/S_L, which leads to an augmentation in the magnitudes of the mean values of $G_2^{11} = (\omega_2\omega_2 + \omega_3\omega_3)/4$ and $G_2^{22} = (\omega_1\omega_1 + \omega_3\omega_3)/4$ from case A to case E. The terms G_3^{11} and G_3^{22} arising from the correlation between pressure and density gradients act as source terms in the transport equations of S_{11} and S_{22}, respectively. The thermal expansion within the flame gives rise to negative values of density gradient and pressure gradient in the flame normal direction, which gives rise to positive mean values of G_3^{11} and G_3^{22}. The relative alignment of density and pressure gradients within the flame front have been discussed elsewhere[27] along with detailed physical explanations, which are not repeated here for the sake of brevity. The pressure Hessian terms G_4^{11}

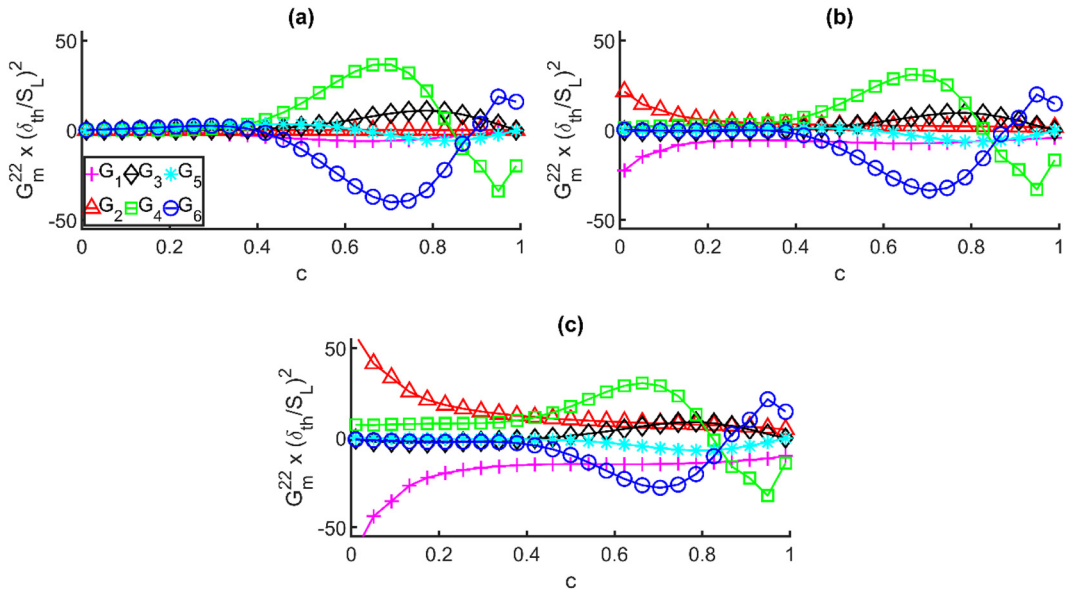

FIG. 4. Same as Fig. 3 but for $\{G_1^{22}, G_2^{22}, G_3^{22}, G_4^{22}, G_5^{22}, G_6^{22}\} \times \delta_{th}^2/S_L^2$ for cases (a) A, (b) C, and (c) E.

and G_4^{22} assume positive mean values for a major part of the flame before exhibiting negative values toward the burned gas side of the flame front. In a steady state laminar flame, the pressure attains its minimum value within the flame, which leads to a negative pressure gradient toward the unburned gas side before assuming positive values toward the burned gas side. This pressure gradient distribution induces negative (positive) values for the second spatial derivative of pressure toward the unburned (burned) gas side of the flame front and accordingly the pressure Hessian terms G_4^{11} and G_4^{22} assume positive (negative) values on the unburned (burned) gas sides of the flame. The behavior of the mean pressure Hessian term in the turbulent cases remains qualitatively similar to that in the case of a steady laminar flame. The magnitudes of the mean values of the pressure Hessian terms G_4^{11} and G_4^{22} remain much higher compared to that of the strain rate contributions (i.e., G_1^{11} and G_1^{22}) and vorticity contributions (i.e., G_2^{11} and G_2^{22}) for case A but magnitudes of the mean values of the pressure Hessian, strain rate, and vorticity contributions become comparable for flames with higher values of Karlovitz number (e.g., case E). The contributions of the mean molecular diffusion and dissipation term G_6^{11} and G_6^{22} behave just opposite to the mean pressure Hessian contributions G_4^{11} and G_4^{22} but the magnitudes of the mean values of G_6^{11} and G_6^{22} remain comparable to the mean values of G_4^{11} and G_4^{22}, respectively. The magnitudes of the mean values of the term originating from the correlations of the density and viscous stress gradients G_5^{11} and G_5^{22} remain small in comparison with the magnitudes of the mean values of $G_1^{11}, G_2^{11}, G_4^{11}, G_6^{11}$ and $G_1^{22}, G_2^{22}, G_4^{22}, G_6^{22}$, respectively. The mean values of the terms G_5^{11} and G_5^{22} assume relatively significant negative values only toward the burned gas side of the flame.

The strengthening of the strain rate and vorticity contributions and the weakening of the pressure Hessian contributions with the increase in *Ka* for the diagonal components are consistent with previous DNS findings[27] for principal strain rate transports for this dataset. However, the principal strain rate directions are not aligned with the Cartesian coordinate directions and thus a direct quantitative comparison with the terms of the transport equations of the diagonal elements of the strain rate tensor is not possible. The weak contributions of the pressure Hessian term in comparison with the strain rate and vorticity contributions to the transport of the diagonal elements of strain rate are also consistent with previous experimental[26] and DNS[27] findings for the principal strain rate transport.

A comparison between Figs. 3 and 4 reveals that the magnitudes of the mean values of the terms of the transport equation for S_{11}, especially the pressure Hessian and dissipation terms, in case A remain smaller than that of the corresponding terms in the transport equation for S_{22} (and also for S_{33} but not explicitly shown here). However, this tendency diminishes with an increase in *Ka* and the terms of the transport equations of S_{11} and S_{22} (and also for S_{33} but not shown here) remain comparable for cases C–E. This suggests that the terms of the strain rate transport exhibit anisotropy for turbulent premixed flames for small values of *Ka* but the extent of this anisotropy decreases with increasing Karlovitz numbers. This behavior was observed also for subgrid/Reynolds stresses and interested readers are referred to Refs. 8, 25, and 52–54 for further information in this regard in terms of Lumley's triangle, which is not repeated here for the sake of conciseness.

The sum of the corresponding terms of the transport equations of the diagonal components of the strain rate tensor provides the terms for the transport equation for dilatation rate $\partial u_i/\partial x_i$ [see Eq. (2)]. Thus, the statistical behaviors of the mean values of G_α^{11}, G_α^{22} and G_α^{33} (for $\alpha = 1, 2\ldots, 6$) provide insights into the mean behaviors of the terms on the right-hand side of Eq. (2). Figures 3 and 4 indicate that the evolution of $\partial u_i/\partial x_i$ is significantly affected by strain rate, vorticity, molecular dissipation, and pressure Hessian contributions but the relative influence of pressure Hessian weakens with increasing *Ka*.

For the sake of completeness, the normalized mean values of the terms on the right side of the transport equations of non-diagonal strain rate components S_{12} and S_{23} (i.e., $\{G_1^{12}, G_2^{12}, G_3^{12}, G_4^{12}, G_5^{12}, G_6^{12}\} \times \delta_{th}^2/S_L^2$ and $\{G_1^{23}, G_2^{23}, G_3^{23}, G_4^{23}, G_5^{23}, G_6^{23}\} \times \delta_{th}^2/S_L^2$) conditioned upon c for cases A, C, and E are shown in Figs. 5 and 6, respectively. The terms of the transport equation of S_{13} are both qualitatively and quantitatively same as that of S_{12} because x_2 and x_3 directions are statistically similar for the canonical configuration considered here. Thus, the terms of the transport equation of S_{13} are not explicitly shown here.

A comparison between Figs. 3–6 reveals that the magnitudes of the mean values of the terms for the non-diagonal strain rate components are smaller (almost by an order of magnitude) than those of the diagonal strain rate components. However, the magnitudes of the mean values of the terms in the transport equation of the non-diagonal strain rate components remain non-negligible, indicating that the principal strain rate directions do not necessarily coincide with the Cartesian coordinates. The mean values of the terms due to pressure Hessian (i.e., G_4^{12} and G_4^{23}), correlation between density and pressure gradients (i.e., G_3^{12} and G_3^{23}), and the combined molecular diffusion and dissipation (i.e., G_6^{12} and G_6^{23}) remain as the significant contributors in case A. In this case, the mean values of the pressure Hessian contributions (i.e., G_4^{12} and G_4^{23}) assume positive (negative) mean values toward the unburned (burned) gas side of the flame and just the opposite behavior was observed for the combined molecular diffusion and dissipation terms (i.e., G_6^{12} and G_6^{23}). However, the qualitative behaviors of the mean values of the pressure Hessian (i.e., G_4^{12} and G_4^{23}) and combined molecular diffusion and dissipation terms (i.e., G_6^{12} and G_6^{23}) change for cases B–E (B and D not shown) where the mean values of G_4^{12} and G_4^{23} assume predominantly negative mean values for the major portion of the flame before exhibiting positive mean values toward the burned gas side. By contrast, the combined molecular diffusion and dissipation term shows predominantly positive mean values for the major portion of the flame before exhibiting negative mean values toward the burned gas side. The mean contributions of the strain rate (i.e., G_1^{12} and G_1^{23}) and vorticity terms (i.e., G_2^{12} and G_2^{23}) to the transports of the non-diagonal strain rate components S_{12} and S_{23} strengthen with increasing *Ka*. The effects of thermal expansion are relatively strong for small values of *Ka* (e.g., in case A), which induces stronger anisotropy in the flow field and this influence is particularly strong in the direction of mean flame propagation. This makes the mean behaviors of the terms of the transport equation of S_{12} and S_{13} in case A differ from that in cases C–E.

It is important to note that the terms of the transport equations of s_α, s_β, and s_γ are presented and their statistical behaviors have been explained elsewhere[27] and the interested readers are referred to Kasten *et al.*[27] for further information in this regard. This information plays a key role in explaining the statistical behaviors of the terms in the $\tilde{E}$ transport equation which will be discussed next. The variations of $\{T_1, T_2, T_3, T_4, T_5, T_6\} \times \delta_{th}^3/\mu_0 S_L^3$ with $\tilde{c}$ for cases A, C, and E are shown in Figs. 7(a)–7(c), respectively.

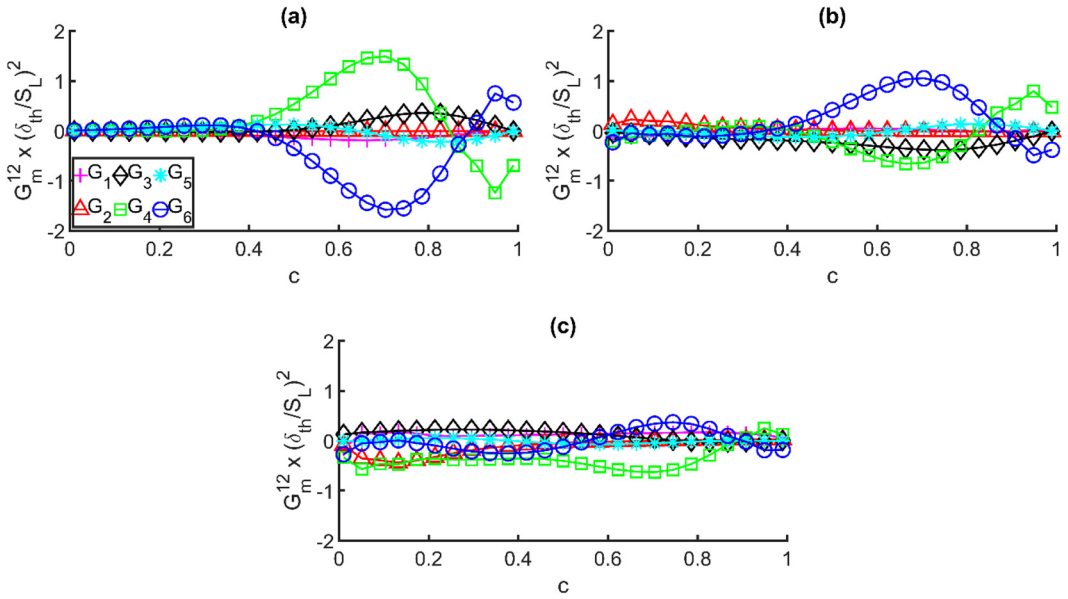

FIG. 5. Same as Fig. 3 but for $\{G_1^{12}, G_2^{12}, G_3^{12}, G_4^{12}, G_5^{12}, G_6^{12}\} \times \delta_{th}^2/S_L^2$ for cases (a) A, (b) C, and (c) E.

It can be seen from Figs. 7(a)–7(c) that the term T_6 acts as a leading order sink in the dissipation rate transport for all cases irrespective of Ka. The terms due to the correlation between density and pressure gradients, and pressure Hessian (i.e., T_3 and T_4) act as the major sources to the Favre-averaged dissipation rate $\tilde{E}$ for case A (and also in case B but not shown here) but these terms become insignificant in comparison with the magnitudes of T_6 for flames with $Ka \gg 1$ (e.g., case E). Moreover, the strain rate term T_1 acts as a sink term in case A throughout the flame brush (and also for the major part of the flame brush in case B except for the leading edge of the flame brush but not shown here), whereas T_1 becomes the leading source term for flames with $Ka \gg 1$ (e.g., case E). However, in case C, the strain rate contribution assumes high positive values toward the unburned gas side of the flame brush, but it becomes weakly negative for $\tilde{c} > 0.4$, and in this case the pressure Hessian term T_4 continues to play an important role as a leading order source term. The magnitude of the vorticity

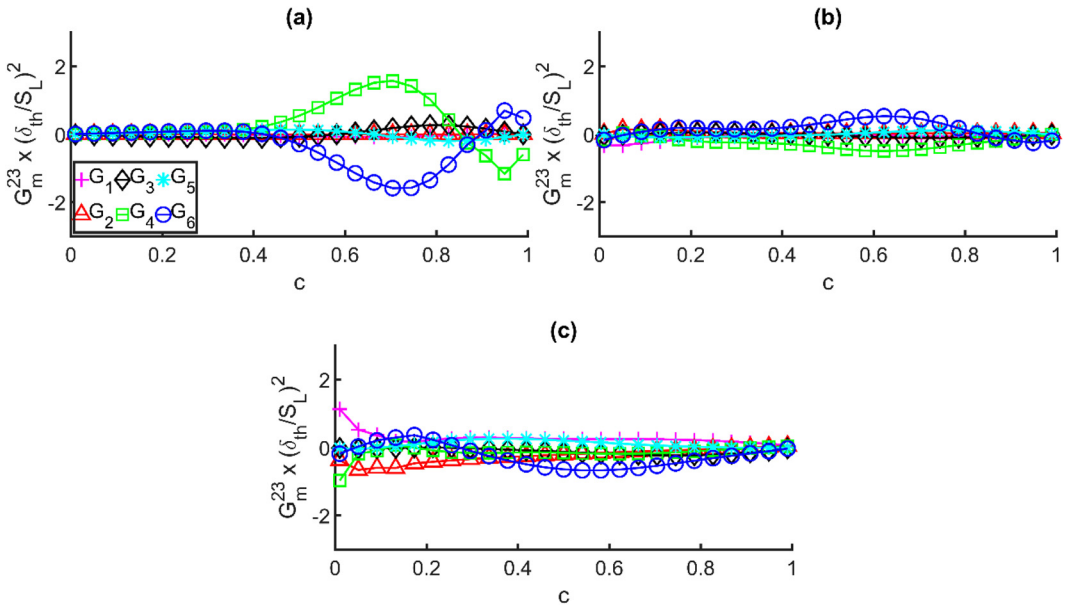

FIG. 6. Same as Fig. 3 but for $\{G_1^{23}, G_2^{23}, G_3^{23}, G_4^{23}, G_5^{23}, G_6^{23}\} \times \delta_{th}^2/S_L^2$ for cases (a) A, (b) C, and (c) E.

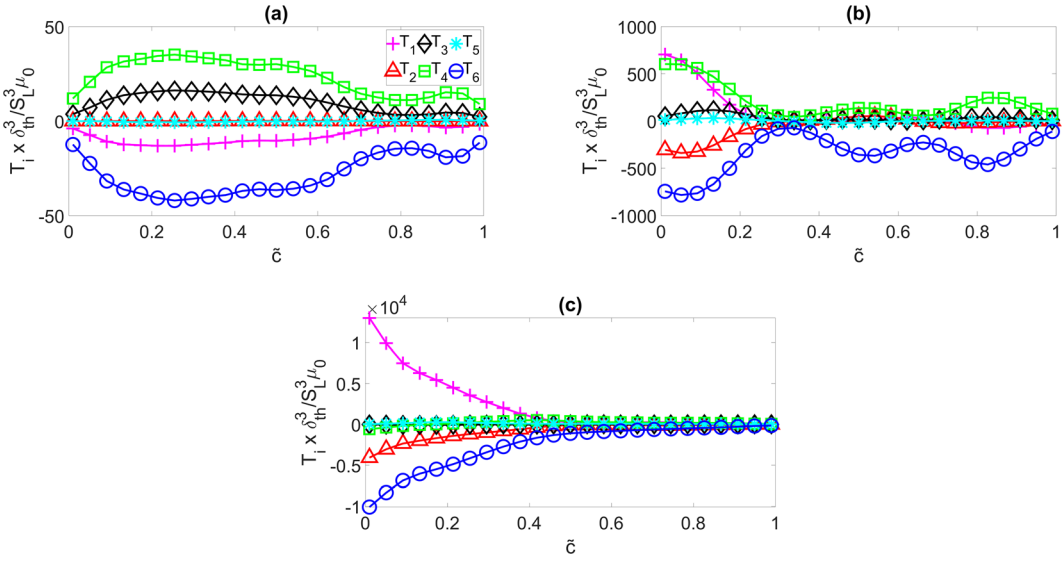

FIG. 7. Variations of $\{T_1, T_2, T_3, T_4, T_5, T_6\} \times \delta_{th}^3/\mu_0 S_L^3$ with $\tilde{c}$ for cases (a) A, (b) C, and (c) E.

contribution T_2 remains negligible in comparison with the terms T_3, T_4, and T_6 in case A. However, T_2 assumes negative values and plays a significant role toward the unburned gas side of the flame brush before becoming insignificant in comparison with the magnitudes of T_3, T_4, and T_6 in cases C–E. The term T_5 arising from the correlations of density and viscous stress gradients remains small in magnitude in comparison with the leading order contributors (e.g., T_6) to the Favre-averaged dissipation rate $\tilde{E}$ transport for all cases, which is consistent with the behavior of G_5^{ij} presented in Figs. 3–6. For flames with $Ka \gg 1$, the leading order balance is maintained between T_1 and T_6 similar to non-reacting flows,[40] and the influence of T_3 and T_4 weakens with increasing Karlovitz number, which is consistent with the observations made from Figs. 3–6 regarding the transport of individual strain rate components. However, for $Ka \gg 1$ flames, the magnitudes of the leading order contributions of T_1, T_2, and T_6 decrease from the unburned to the burned gas side of the flame brush.

The term T_1 can be written as $T_1 = -4\mu(s_\alpha^3 + s_\beta^3 + s_\gamma^3) + 4\mu(s_\alpha^2 + s_\beta^2 + s_\gamma^2)(s_\alpha + s_\beta + s_\gamma)/3$ where s_α, s_β and s_γ are the most extensive (or most positive), intermediate and the most compressive (or most negative) principal strain rate, respectively. For case A, $s_\alpha \gg s_\beta$ and $s_\alpha \gg |s_\gamma|$ (see Fig. 2), and thus, T_1 assumes negative values in this case. However, in case E, $|s_\gamma| > s_\alpha > s_\beta$ (see Fig. 2), as in the case of non-reacting flows,[55,56] which leads to positive values of T_1. For case C, $|s_\gamma| > s_\alpha > s_\beta$ is maintained toward the unburned gas side of the flame, where the effects of heat release are weak and therefore T_1 assumes positive values in this region. However, the magnitudes of s_α and s_γ become comparable in the middle of the flame brush in case C, which results in small negative values of T_1. The tendency obtaining $|s_\gamma| > s_\alpha > s_\beta$ (see Fig. 2), as in the case of non-reacting flows,[55,56] increases with increasing Ka, and therefore the likelihood of obtaining positive value of T_1 increases with an increase in Ka.

Based on the eigendecomposition, T_2 can be expressed as: $T_2 = \overline{\mu s_\alpha(\hat{\omega}_\beta\hat{\omega}_\beta + \hat{\omega}_\gamma\hat{\omega}_\gamma - 2\hat{\omega}_\alpha\hat{\omega}_\alpha)/3} + \overline{\mu s_\beta(\hat{\omega}_\alpha\hat{\omega}_\alpha + \hat{\omega}_\gamma\hat{\omega}_\gamma - 2\hat{\omega}_\beta\hat{\omega}_\beta)/3} + \overline{\mu s_\gamma(\hat{\omega}_\alpha\hat{\omega}_\alpha + \hat{\omega}_\beta\hat{\omega}_\beta - 2\hat{\omega}_\gamma\hat{\omega}_\gamma)/3}$[18] where $\hat{\omega}_\alpha, \hat{\omega}_\beta$, and $\hat{\omega}_\gamma$ are the components of vorticity in the directions of the most extensive, intermediate and the most compressive principal strain rate directions, respectively. It was shown in previous studies[16,27] that $\vec{\omega}$ preferentially aligns with the intermediate principal strain rate direction irrespective of the combustion regime but the alignment of $\vec{\omega}$ with the most extensive and most compressive eigendirections changes depending on the regime of combustion.[16,27] For the combination of small Ka (i.e., $Ka < 1$) and large Da (i.e., $Da > 1$), such as in case A, $\vec{\omega}$ does not show any alignment with the most extensive principal strain rate eigendirection but a significant amount of collinear alignment with the eigendirection associated with the most compressive principal strain rate (shown in Ref. 27 for this database), which leads to $\hat{\omega}_\beta\hat{\omega}_\beta \gg \hat{\omega}_\alpha\hat{\omega}_\alpha$ and $\hat{\omega}_\gamma\hat{\omega}_\gamma \gg \hat{\omega}_\alpha\hat{\omega}_\alpha$. By contrast, for $Ka > 1$ and $Da < 1$ flames (e.g., cases C–E), $\vec{\omega}$ exhibits significant collinear alignment with the eigendirection associated with s_α, which was shown in Ref. 27 for this database. This leads to $\hat{\omega}_\beta\hat{\omega}_\beta \gg \hat{\omega}_\gamma\hat{\omega}_\gamma$ and $\hat{\omega}_\alpha\hat{\omega}_\alpha \gg \hat{\omega}_\gamma\hat{\omega}_\gamma$ for $Ka > 1$ and $Da < 1$ flames (e.g., cases C–E). The explanations for the above behaviors are provided elsewhere[16,27] and thus are not repeated here. These vorticity alignment characteristics with strain rate eigendirections suggest that $\overline{\mu s_\alpha(\hat{\omega}_\beta\hat{\omega}_\beta + \hat{\omega}_\gamma\hat{\omega}_\gamma - 2\hat{\omega}_\alpha\hat{\omega}_\alpha)/3}$ is the dominant contributor to T_2 in case A, whereas $\overline{\mu s_\gamma(\hat{\omega}_\alpha\hat{\omega}_\alpha + \hat{\omega}_\beta\hat{\omega}_\beta - 2\hat{\omega}_\gamma\hat{\omega}_\gamma)/3}$ is the major contributor to T_2 in cases C–E (also in case B but not shown here). However, the magnitude of $\vec{\omega}$ remains small in case A, as suggested by the small magnitudes of G_2^{ij} in Figs. 3–6. This leads to a negligible contribution of T_2 in case A. The negative value of s_γ leads to a negative value of T_2 in cases C–E. As the magnitude of $\vec{\omega}$ decreases from the unburned to the burned gas side, the magnitude of T_2 drops with the increasing $\tilde{c}$ in cases C–E (also in case B but not shown here).

The term T_3 can be written as $T_3 = \overline{4\mu(s_\alpha G_3^\alpha + s_\beta G_3^\beta + s_\gamma G_3^\gamma)} - \overline{4\mu(G_3^\alpha + G_3^\beta + G_3^\gamma)(s_\alpha + s_\beta + s_\gamma)/3}$, which leads to $T_3 = \overline{(4\mu/3)[G_3^\alpha(3s_\alpha - \partial u_i/\partial x_i) + G_3^\beta(3s_\beta - \partial u_i/\partial x_i) + G_3^\gamma(3s_\gamma - \partial u_i/\partial x_i)]}$ with G_3^α, G_3^β and G_3^γ being the components of the tensor G_3^{ij} in the

principal strain rate eigendirections corresponding to the most extensive, intermediate, and the most compressive principal strain rate directions, respectively. It was demonstrated in a previous analysis[27] that G_3^{α},G_3^{β}, and G_3^{γ} assume predominantly positive values because both pressure and density drop within the flame and ∇p and $\nabla \rho$ show collinear alignment with ∇c in these flames (see Figs. 3 and 11 in Ref. 27). In case A, $G_3^{\alpha} \gg G_3^{\beta}$ and $G_3^{\alpha} \gg G_3^{\gamma}$ are obtained because both ∇p and $\nabla \rho$ show collinear alignment with the eigendirection associated with s_{α} (see Figs. 4 and 8 in Ref. 27), which suggests that $\overline{(4\mu/3)[G_3^{\alpha}(3s_{\alpha}-\partial u_i/\partial x_i)}$ is the dominant contributor to T_3 in this case. As $s_{\alpha} \approx \partial u_i/\partial x_i$ in case A (see Fig. 2), $\overline{(4\mu/3)[G_3^{\alpha}(3s_{\alpha}-\partial u_i/\partial x_i)}$ yields a relatively strong positive contribution of T_3. A qualitatively similar behavior is also observed in case B (not shown here). However, in other cases, the positive contribution of $\overline{(4\mu/3)[G_3^{\alpha}(3s_{\alpha}-\partial u_i/\partial x_i)}$ is nullified by the negative values of $\overline{(4\mu/3)[G_3^{\gamma}(3s_{\gamma}\partial u_i/\partial x_i)}$, which leads to a relatively weak contribution of T_3 in flames with $Ka > 1$ and $Da < 1$ (e.g., cases C–E).

The pressure Hessian contribution T_4 can be expressed as $T_4 = \overline{(4\mu/3)[s_{\alpha}(2G_4^{\alpha}-G_4^{\beta}-G_4^{\gamma})+s_{\beta}(2G_4^{\beta}-G_4^{\alpha}-G_4^{\gamma})+s_{\gamma}(2G_4^{\gamma}-G_4^{\beta}-G_4^{\gamma})]}$, where G_4^{α},G_4^{β}, and G_4^{γ} are the components of the tensor G_3^{ij} in the principal strain rate eigendirections corresponding to the most extensive, intermediate, and the most compressive principal strain rate directions, respectively. The components G_4^{α},G_4^{β},andG_4^{γ} are given by

$$G_4^{\alpha} = \Pi_{\alpha}\cos^2(\hat{\pi}_{\alpha},\hat{e}_{\alpha}) + \Pi_{\beta}\cos^2(\hat{\pi}_{\beta},\hat{e}_{\alpha}) + \Pi_{\gamma}\cos^2(\hat{\pi}_{\gamma},\hat{e}_{\alpha}), \quad (7a)$$

$$G_4^{\beta} = \Pi_{\alpha}\cos^2(\hat{\pi}_{\alpha},\hat{e}_{\beta}) + \Pi_{\beta}\cos^2(\hat{\pi}_{\beta},\hat{e}_{\beta}) + \Pi_{\gamma}\cos^2(\hat{\pi}_{\gamma},\hat{e}_{\beta}), \quad (7b)$$

$$G_4^{\gamma} = \Pi_{\alpha}\cos^2(\hat{\pi}_{\alpha},\hat{e}_{\gamma}) + \Pi_{\beta}\cos^2(\hat{\pi}_{\beta},\hat{e}_{\gamma}) + \Pi_{\gamma}\cos^2(\hat{\pi}_{\gamma},\hat{e}_{\gamma}), \quad (7c)$$

where Π_{α}, Π_{β}, and Π_{γ} are the most extensive, intermediate, and the most compressive eigenvalues of $\partial^2 p/\partial x_i \partial x_j$ with $\hat{\pi}_{\alpha}$, $\hat{\pi}_{\beta}$, and $\hat{\pi}_{\gamma}$ being the corresponding eigenvectors, and $\hat{e}_{\alpha}$, $\hat{e}_{\beta}$, and $\hat{e}_{\gamma}$ are the strain rate eigenvectors corresponding to s_{α}, s_{β}, and s_{γ}, respectively. It was shown by Kasten *et al.*[27] that for case A $\hat{e}_{\alpha}$, $\hat{e}_{\beta}$ and $\hat{e}_{\gamma}$ preferentially align collinearly with $\hat{\pi}_{\gamma}$, $\hat{\pi}_{\beta}$, and $\hat{\pi}_{\alpha}$, respectively, within a major part of the flame but toward the burned gas side $\hat{e}_{\alpha}$, $\hat{e}_{\beta}$, and $\hat{e}_{\gamma}$ remain aligned with $\hat{\pi}_{\alpha}$, $\hat{\pi}_{\gamma}$, and $\hat{\pi}_{\beta}$, respectively. Although these trends are observed for moderate turbulence intensities (e.g., cases B and C), the extent of these alignments decreases with the increasing u'/S_L. The alignments between $\hat{e}_{\alpha}$ with $\hat{\pi}_{\gamma}$ and between $\hat{e}_{\gamma}$ with $\hat{\pi}_{\alpha}$ yield large positive values of G_4^{α} and G_4^{γ} within the reaction zone but the perfect alignment between $\hat{e}_{\alpha}$, $\hat{e}_{\beta}$ and $\hat{e}_{\gamma}$ with $\hat{\pi}_{\alpha}$, $\hat{\pi}_{\gamma}$, and $\hat{\pi}_{\beta}$, respectively, leads to negative values of G_4^{α} and G_4^{γ} toward the burned gas side for cases A and B. Moreover, this leads to small magnitudes of G_4^{β} in comparison with G_4^{α} and G_4^{γ} for cases A and B. For non-reacting isotropic turbulent flows, $\hat{e}_{\alpha}$ and $\hat{e}_{\gamma}$ are in incomplete alignment with $\hat{\pi}_{\alpha}$ and $\hat{\pi}_{\gamma}$, whereas $\hat{e}_{\beta}$ and $\hat{\pi}_{\beta}$ are collinearly aligned, whereas under anisotropic turbulence, $\hat{e}_{\alpha}$ and $\hat{e}_{\gamma}$ exhibit incomplete alignment with $\hat{\pi}_{\alpha}$ and $\hat{\pi}_{\beta}$, but a perfect alignment is obtained between $\hat{e}_{\beta}$ and $\hat{\pi}_{\gamma}$.[27] The incomplete alignments between $\hat{e}_{\alpha}$ ($\hat{e}_{\gamma}$) and $\hat{\pi}_{\alpha}$ ($\hat{\pi}_{\gamma}$) are also obtained for cases D and E, similar to non-reacting flows,[57,58] and these imperfect alignments give rise to reduced relative importance of G_4^{α}, G_4^{β}, and G_4^{γ} for high turbulence intensities.[27] However, the collinear alignment of $\hat{e}_{\alpha}$ and $\hat{e}_{\gamma}$ with $\hat{\pi}_{\gamma}$, and $\hat{\pi}_{\alpha}$, respectively, increases in the heat releasing zone of the flame even for cases D and E, and this leads to positive values of G_4^{α}, G_4^{β}, and G_4^{γ} for $0.5 \leq c \leq 0.8$.[27] The behaviors of G_4^{α} and G_4^{γ} are found to be mostly qualitatively similar to G_{11} and G_{22} in Figs. 3 and 4. The combination of $s_{\alpha} > |s_{\beta}|$, $s_{\alpha} > |s_{\gamma}|$, $|G_4^{\alpha}| > |G_4^{\beta}|$, and $|G_4^{\gamma}| > |G_4^{\beta}|$ in case A gives rise to a significant positive contribution of $T_4 = \overline{(4\mu/3)[s_{\alpha}(2G_4^{\alpha}-G_4^{\beta}-G_4^{\gamma})+s_{\beta}(2G_4^{\beta}-G_4^{\alpha}-G_4^{\gamma})+s_{\gamma}(2G_4^{\gamma}-G_4^{\beta}-G_4^{\gamma})]}$ in case A (and also in case B) because G_4^{α} and G_4^{γ} assume positive values for the major part of the flame brush. However, the magnitudes of s_{α},s_{β}, and s_{γ} are comparable (see Fig. 2) and the same holds for G_4^{α},G_4^{β}, and G_4^{γ} for high turbulence intensities[27] and thus positive and negative contributions of $\overline{(4\mu/3)s_{\alpha}(2G_4^{\alpha}-G_4^{\beta}-G_4^{\gamma})}$, $\overline{(4\mu/3)s_{\beta}(2G_4^{\beta}-G_4^{\alpha}-G_4^{\gamma})}$, and $\overline{(4\mu/3)s_{\gamma}(2G_4^{\gamma}-G_4^{\beta}-G_4^{\gamma})}$ mostly nullify each other to yield relatively weak magnitude of T_4 in comparison with T_1.

It has been found that the magnitudes of G_5^{ij} remain small in comparison with the leading order source/sink terms of the transport equations of S_{ij}, and therefore, the magnitudes of T_5 are found to be negligible in comparison with the leading order source and sink terms of the transport equation of $\tilde{E}$ for all cases. The term T_6 can be decomposed as

$$T_6 = \underbrace{\overline{4\rho\nu^2\left(S_{ij}-\frac{\delta_{ij}}{3}\right)\left(\frac{\partial^2 S_{mm}}{\partial x_i \partial x_j}\right)}}_{T_{6(i)}} + \underbrace{\overline{\frac{\partial}{\partial x_j}\left(\mu\frac{\partial E}{\partial x_j}\right)}}_{T_{6(ii)}} \underbrace{-\overline{4\rho\nu^2\left(\frac{\partial S_{ij}}{\partial x_k}\frac{\partial S_{ij}}{\partial x_k}-\frac{1}{3}\frac{\partial S_{ll}}{\partial x_k}\frac{\partial S_{mm}}{\partial x_k}\right)}}_{T_{6(iii)}}. \quad (8)$$

The term $T_{6(iii)}$ is a negative semi-definite term (i.e., $T_{6(iii)} \leq 0$) because of the mathematical identity $[(\partial S_{ij}/\partial x_k)(\partial S_{ij}/\partial x_k) - 1/3(\partial S_{ll}/\partial x_k)(\partial S_{mm}/\partial x_k)] > 0$ and in the context of RANS, $|T_{6(ii)}| \ll |T_{6(iii)}|$. The term $\partial^2 S_{mm}/\partial x_n \partial x_n$ changes the sign within the flame and positive and negative values are equally likely for $\partial^2 S_{mm}/\partial x_t \partial x_t$ (where subscripts n and t are used for flame normal and tangential directions, respectively), and therefore, the net contribution of $T_{6(i)}$ remains much smaller in magnitude in comparison with $T_{6(iii)}$ (i.e., $|T_{6(i)}| \ll |T_{6(iii)}|$) for all cases. This suggests that T_6 assumes negative values for all cases due to negative semi-definite values of $T_{6(iii)}$.

Finally, it is worthwhile to consider the scaling estimates of the terms $T_1 - T_6$. The timescale associated with the fluctuating strain rate is scaled with respect to a timescale t_s given by: $t_s^{-1} = \max(S_L/\delta_{th}, u'/\Lambda) \sim (S_L/\delta_{th})\max\{1, Ka\}$ where the strain rate is expected to be dominated by the chemical timescale in the corrugated flamelets regime (i.e., $Ka < 1$),[1] whereas in the thin reaction zones regime the fluctuating strain rate can be scaled using u'/Λ following Tennekes and Lumley[59] where Λ is the Taylor micro-scale. The fluctuating vorticity components can also be scaled as: u'/Λ following Tennekes and Lumley.[59] In addition, if the density and pressure gradients and the second-derivative of pressure are scaled using ρ_0/δ_{th}, $\tau\rho_0 S_L^2/\delta_{th}$, and $\tau\rho_0 S_L^2/\delta_{th}^2$, respectively, following Steinberg *et al.*,[26] it is possible to obtain the following scaling estimates:

$$T_1 \sim \mu_0 t_s^{-3}, \quad T_2 \sim \mu_0 t_s^{-1}\left(u'^2/\Lambda^2\right), \quad T_3 \sim \mu_0 t_s^{-1}\left(\tau S_L^2/\delta_{th}^2\right),$$
$$T_4 \sim \mu_0 t_s^{-1}\left(\tau S_L^2/\delta_{th}^2\right), \quad T_5 \sim \mu_0 t_s^{-2}(S_L/\delta_{th})(\delta_{th}/l_d), \quad (9)$$
$$T_6 \sim \mu_0 t_s^{-2}(S_L/\delta_{th})\left(\delta_{th}^2/l_d^2\right),$$

where l_d is a length scale associated with the strain rate gradients, which is taken to be $l_d \sim \max(\delta_{th}, \eta) \sim \delta_{th}\max(1, Ka^{-0.5})$ (where η is the Kolmogorov length scale) because the largest strain rate gradient is expected to be associated with δ_{th} and η in the corrugated flamelets (i.e., $Ka < 1$) and thin reaction zones (i.e., $Ka > 1$) regimes, respectively. According to Eq. (9), T_1, T_3, T_4, and T_6 are expected to play leading order roles in the corrugated flamelets regime (i.e., $Ka < 1$), and are expected to be of the order of $\mu_0 S_L^3/\delta_{th}^3$, which is consistent with the observations made for case A in Fig. 7. By contrast, T_1, T_2, and T_6 become the leading order terms in the thin reaction zones regime (i.e., $Ka > 1$) flames, and scale as $\mu_0 S_L^3/\delta_{th}^3 \times Ka^3$, which is consistent with the observations made from Fig. 7 for cases C–E. For the thin reaction zones regime (i.e., $Ka > 1$) flames, the terms T_3 and T_4 scale as $\tau\mu_0 S_L^3/\delta_{th}^3 \times Ka$, and therefore, these terms remain negligible in comparison with the magnitudes of T_1, T_2 and T_6 in cases C–E. These scaling estimates are also consistent with an increase in the magnitudes of terms of the transport equation of $\tilde{E}$ with an increase in Ka.

The two-equation model for turbulent fluid motion solves a transport equation for the dissipation rate of turbulent kinetic energy and the same holds true for Reynolds stress closures. However, this equation is also unclosed and requires modeling. The present analysis of the dissipation rate transport equation, and the scaling analysis suggests that the leading order terms that need to be modeled most accurately change depending on the regime of premixed combustion (i.e., on the value of Karlovitz number). It also indicates that the alignments of vorticity and pressure Hessian with strain rate eigenvectors change depending on the regime of combustion. For large Karlovitz numbers, they resemble those of non-reacting turbulent flows, but significant differences are to be expected for small Karlovitz numbers due to the significant contributions of the density variation and pressure Hessian terms in the dissipation rate transport equation, which do not play leading order roles for high values of Karlovitz number.

IV. CONCLUSIONS

The statistical behaviors of the evolutions of the components of the strain rate tensor and Favre-averaged dissipation rate of kinetic energy have been analyzed for different turbulence intensities spanning a range of different Karlovitz numbers using DNS data of statistically planar turbulent premixed flames propagating into forced unburned gas turbulence. The mean direction of flame propagation is taken to align with the x_1-direction. Consequently, the magnitudes of the terms of the transport equations of the diagonal components of the strain rate tensor remain much greater than the corresponding terms of the non-diagonal components of the strain rate tensor within the flame. It has been found that the pressure Hessian contribution and the combined molecular diffusion and dissipation terms remain the dominant contributors and the magnitudes of their mean values remain greater than the strain rate and vorticity contributions in the transport equations of the diagonal strain rate components and Favre-averaged dissipation rate of kinetic energy for flames with small turbulence intensities characterized by $Da > 1$ and $Ka < 1$. However, the leading order balance is maintained between the strain rate, vorticity, and molecular dissipation contributions for flames with $Da < 1$ and $Ka > 1$, similar to non-reacting turbulent flows. The contributions of the terms arising from the correlation between pressure and density gradients and pressure Hessian to the strain rate and dissipation rate of kinetic energy transports are found to weaken in comparison to the corresponding molecular dissipation contributions with an increase in Ka. Detailed physical explanations have been provided in terms of alignments of vorticity, pressure gradient, and pressure Hessian eigenvectors with principal strain rate directions for the changes in relative importances of different terms of the transport equations of strain rate components and the Favre-averaged dissipation rate of kinetic energy. The magnitudes of the terms of the Favre-averaged dissipation rate of kinetic energy increase with the increasing Ka, which has been explained with the help of a detailed scaling analysis. The scaling analysis has also been utilized to identify the leading order contributions to the dissipation rate of kinetic energy for different combustion regimes. Although the present analysis focuses on fluid-dynamical aspects and previous findings from simple and detailed chemistry cases revealing qualitatively similar enstrophy transport statistics,[17–19] the present findings based on simple chemistry need to be validated in the future in the context of detailed chemistry and transport. Moreover, the modeling of the unclosed terms of the Favre-averaged dissipation rate of kinetic energy will form the foundation for future analyses.

ACKNOWLEDGMENTS

The authors are grateful to EPSRC for the financial support, and the computational support was provided by ARCHER (EP/R029369/1), CIRRUS, Leibniz Supercomputing Centre (Grant No. pn69ga), and Rocket-HPC.

AUTHOR DECLARATIONS

Conflict of Interest

The authors have no conflicts to disclose.

DATA AVAILABILITY

The data that support the findings of this study are available from the corresponding author upon reasonable request.

REFERENCES

[1]N. Peters, *Turbulent Combustion, Cambridge Monograph on Mechanics* (Cambridge University Press, Cambridge, 2000).
[2]D. Veynante and L. Vervisch, "Turbulent combustion modelling," Prog. Energy Combust. Sci. **28**, 193 (2002).
[3]A. Lipatnikov, *Fundamentals of Premixed Turbulent Combustion* (Taylor and Francis, 2013).
[4]M. Klein, M. Pfitzner, N. Chakraborty, and F. Creta, "Workshop on fundamental understanding and modelling of high pressure turbulent premixed combustion," Combust. Sci. Technol. **192**, 1997 (2020).
[5]N. Swaminathan and K. Bray, *Turbulent Premixed Flames* (Cambridge University Press, Cambridge, 2011).
[6]A. N. Lipatnikov and J. Chomiak, "Turbulent flame speed and thickness: Phenomenology, evaluation, and application in multi-dimensional simulations," Prog. Energy Combust. Sci. **28**, 1–74 (2002).
[7]A. N. Lipatnikov and J. Chomiak, "Effects of premixed flames on turbulence and turbulent scalar transport," Prog. Energy Combust. Sci. **36**, 1–102 (2010).

[8]N. Chakraborty, "Influence of thermal expansion on fluid dynamics of turbulent premixed combustion and its modelling implications," Flow Turbul. Combust. **106**, 753–848 (2021).
[9]J. F. Driscoll, "Turbulent premixed combustion: Flamelet structure and its effect on turbulent burning velocities," Prog. Energy Combust. Sci. **34**, 91–134 (2008).
[10]A. M. Steinberg, P. E. Hamlington, and X. Zhao, "Structure and dynamics of highly turbulent premixed combustion," Prog. Energy Combust. Sci. **85**, 100900 (2021).
[11]S. Zhang and C. J. Rutland, "Premixed flame effects on turbulence and pressure-related terms," Combust. Flame **102**, 447–461 (1995).
[12]S. D. Mason and C. J. Rutland, "Turbulent transport in spatially developing reacting shear layers," Proc. Combust. Inst. **28**, 505–513 (2000).
[13]S. Nishiki, T. Hasegawa, R. Borghi, and R. Himeno, "Modelling of flame generated turbulence based on direct numerical simulation databases," Proc. Combust. Inst. **29**, 2017–2022 (2002).
[14]N. Chakraborty, M. Katragadda, and R. S. Cant, "Statistics and modelling of turbulent kinetic energy transport in different regimes of premixed combustion," Flow Turbul. Combust. **87**, 205–235 (2011).
[15]N. Chakraborty, M. Katragadda, and R. S. Cant, "Effects of Lewis number on turbulent kinetic energy transport in turbulent premixed combustion," Phys. Fluids **23**, 075109 (2011).
[16]N. Chakraborty, "Alignment of vorticity with strain rates in turbulent premixed flames," Eur. J. Mech. B-Fluids **46**, 201–220 (2014).
[17]A. L. Lipatnikov, S. Nishiki, and T. Hasegawa, "A direct numerical simulation study of vorticity transformation in weakly turbulent premixed flames," Phys. Fluids **26**, 105104 (2014).
[18]N. Chakraborty, I. Konstantinou, and A. Lipatnikov, "Effects of Lewis number on vorticity and enstrophy transport in turbulent premixed flames," Phys. Fluids **28**, 015109 (2016).
[19]V. Papapostolou, D. H. Wacks, M. Klein, N. Chakraborty, and H. G. Im, "Enstrophy transport conditional on local flow topologies in different regimes of premixed turbulent combustion," Sci. Rep. **7**, 11545 (2017).
[20]A. N. Lipatnikov, V. L. Sabelnikov, N. V. Nikitin, S. Nishiki, and T. Hasegawa, "Influence of thermal expansion on potential and rotational components of turbulent velocity field within and upstream of premixed flame brush," Flow Turbul. Combust. **106**(4), 1111 (2021).
[21]N. Chakraborty and N. Swaminathan, "Influence of Damköhler number on turbulence-scalar interaction in premixed flames, Part I: Physical insight," Phys. Fluids **19**, 045103 (2007).
[22]G. Hartung, J. Hult, C. F. Kaminski, J. W. Rogerson, and N. Swaminathan, "Effect of heat release on turbulence and scalar-turbulence interaction in premixed combustion," Phys. Fluids **20**, 035110 (2008).
[23]N. Chakraborty, M. Klein, and N. Swaminathan, "Effects of Lewis number on reactive scalar gradient alignment with local strain rate in turbulent premixed flames," Proc. Combust. Inst. **32**, 1409–1417 (2009).
[24]C. Dopazo, L. Cifuentes, J. Martin, and C. Jimenez, "Strain rates normal to approaching iso-scalar surfaces in a turbulent premixed flame," Combust. Flame **162**, 1729–1736 (2015).
[25]U. Ahmed, M. Klein, and N. Chakraborty, "On the stress-strain alignment in premixed turbulent flames," Sci. Rep. **9**, 5092 (2019).
[26]A. M. Steinberg, B. Coriton, and J. H. Frank, "Influence of combustion on principal strain-rate transport in turbulent premixed flames," Proc. Combust. Inst. **35**, 1287–1296 (2015).
[27]C. Kasten, U. Ahmed, M. Klein, and N. Chakraborty, "Principal strain rate evolution within turbulent premixed flames for different combustion regimes," Phys. Fluids **33**, 015111 (2021).
[28]N. Swaminathan and K. N. C. Bray, "Effect of dilatation on scalar dissipation in turbulent premixed flames," Combust. Flame **143**, 549–565 (2005).
[29]M. Katragadda, S. P. Malkeson, and N. Chakraborty, "Modelling of the tangential strain rate term of the flame surface density transport equation in the context of Reynolds averaged Navier–Stokes simulation," Proc. Combust. Inst. **33**, 1429–1437 (2011).
[30]J. Sellmann, J. Lai, N. Chakraborty, and A. M. Kempf, "Flame surface density based modelling of head-on quenching of turbulent premixed flames," Proc. Combust. Inst. **36**, 1817–1825 (2017).
[31]N. Chakraborty and N. Swaminathan, "Influence of Damköhler number on turbulence-scalar interaction in premixed flames, Part II: Model development," Phys. Fluids **19**, 045104 (2007).
[32]U. Ahmed, R. Prosser, and A. J. Revell, "Towards the development of an evolution equation for flame turbulence interaction in premixed turbulent combustion," Flow Turbul. Combust. **93**, 637–663 (2014).
[33]U. Ahmed and R. Prosser, "Modelling flame turbulence interaction in rans simulation of premixed turbulent combustion," Combust. Theor. Modell. **20**, 34–57 (2016).
[34]G. C. Layek and Sunita, "Non-Kolmogorov scaling and dissipation laws in planar turbulent plume," Phys. Fluids **30**, 115105 (2018).
[35]G. A. Gerolymos and I. Vallet, "Destruction-of-dissipation and time-scales in wall turbulence," Phys. Fluids **31**, 055103 (2019).
[36]Y. Wu, W. Zhang, Y. Wang, Z. Zou, and J. Chen, "Energy dissipation analysis based on velocity gradient tensor decomposition," Phys. Fluids **32**, 035114 (2020).
[37]V. A. Sabelnikov, A. N. Lipatnikov, S. Nishiki, H. L. Dave, F. E. Hernández Pérez, W. Song, and H. G. Im, "Dissipation and dilatation rates in premixed turbulent flames," Phys. Fluids **33**, 035112 (2021).
[38]J. Lemay, L. Djenidi, and R. Antonia, "Estimation of mean turbulent kinetic energy and temperature variance dissipation rates using a spectral chart method," Phys. Fluids **32**, 055109 (2020).
[39]N. Chakraborty, J. W. Rogerson, and N. Swaminathan, "A-priori assessment of closures for scalar dissipation rate transport in turbulent premixed flames using direct numerical simulation," Phys. Fluids **20**, 045106 (2008).
[40]K. K. Nomura and G. K. Post, "The structure and dynamics of vorticity and rate of strain in incompressible homogeneous turbulence," J. Fluid Mech. **377**, 65–97 (1998).
[41]D. C. Wilcox, *Turbulence Modelling for CFD*, 3rd ed. (DCW Industries, 2006).
[42]U. Ahmed, N. Chakraborty, and M. Klein, "Insights into the bending effect in premixed turbulent combustion using the flame surface density transport," Combust. Sci. Technol. **191**, 898–920 (2019).
[43]P. Brearley, U. Ahmed, N. Chakraborty, and A. N. Lipatnikov, "Statistical behaviours of conditioned two-point second-order structure functions in turbulent premixed flames in different combustion regimes," Phys. Fluids **31**, 115109 (2019).
[44]S. K. Lele, "Compact finite difference schemes with spectral like resolution," J. Comput. Phys. **103**, 16–42 (1992).
[45]G. A. Blaisdell, N. N. Mansour, and W. C. Reynolds, "Compressiblity effects on the growth and structure of homogeneous turbulent shear flow," J. Fluid Mech. **256**, 443–485 (1993).
[46]Z.-S. She, E. Jackson, and S. A. Orszag, "Scale-dependent intermittency and coherence in turbulence," J. Sci. Comput. **3**, 407–434 (1988).
[47]G. Batchelor and A. Townsend, "The nature of turbulent motion at large wavenumbers," in *Proceedings of the Royal Society of London A: Mathematical, 240 Physical and Engineering Sciences* (The Royal Society, 1949), Vol. 199, pp. 238–255.
[48]A. S. Monin and A. M. Yaglom, *Statistical Fluid Mechanics, Mechanics of Turbulence* (Courier Corporation, 2013), Vol. 2.
[49]K. Yamamoto and T. Kambe, "Gaussian and near-exponential probability distributions of turbulence obtained from a numerical simulation," Fluid Dyn. Res. **8**, 65–72 (1991).
[50]M. Klein, N. Chakraborty, and S. Ketterl, "A comparison of strategies for Direct Numerical Simulation of turbulence chemistry interaction in generic planar turbulent premixed flames," Flow Turbul. Combust. **99**, 955–971 (2017).
[51]F. B. Keil, M. Amzehnhoff, U. Ahmed, N. Chakraborty, and M. Klein, "Comparison of flame propagation statistics extracted from direct numerical simulation based on simple and detailed chemistry—Part 1: Fundamental flame turbulence interaction," Energies **14**, 5548 (2021).

[52]M. Klein, C. Kasten, and N. Chakraborty, "A-priori direct numerical simulation assessment of models for generalized sub-grid scale turbulent kinetic energy in turbulent premixed flames," Comput. Fluids **154**, 123–131 (2017).
[53]M. Klein, C. Kasten, N. Chakraborty, N. Mukhadiyev, and H. G. Im, "Turbulent scalar fluxes in H_2-air premixed flames at low and high Karlovitz numbers," Combust. Theor. Modell. **22**, 1033–1048 (2018).
[54]P. Brearley, U. Ahmed, N. Chakraborty, and M. Klein, "Scaling of second-order structure functions in turbulent premixed flames in the flamelet combustion regime," Fluids **5**(2), 89 (2020).
[55]W. T. Ashurst, A. R. Kerstein, R. M. Kerr, and C. H. Gibson, "Alignment of vorticity and scalar gradient with strain rate in simulated Navier–Stokes turbulence," Phys. Fluids **30**, 2343 (1987).
[56]T. Poinsot and D. Veynante, *Theoretical and Numerical Combustion* (R.T. Edwards Inc., Philadelphia, PA, 2001).
[57]C. Kalelkar, "Statistics of pressure fluctuations in decaying isotropic turbulence," Phys. Rev. E **73**, 046301 (2006).
[58]J. M. Lawson and J. R. Dawson, "On velocity gradient dynamics and turbulent structure," J. Fluid Mech. **780**, 60–98 (2015).
[59]H. Tennekes and J. L. Lumley, *A First Course in Turbulence*, 1st ed. (MIT Press, 1972).